Yoshihiro Nakata, Atsuhiro Ide, Yutaka Nakamura, Katsuhiro Hirata, and Hiroshi Ishiguro, "Hopping of a monopedal robot with a biarticular muscle driven by electromagnetic linear actuators," 2012 IEEE International Conference on Robotics and Automation, Saint Paul, MN, 2012, pp. 3153-3160. DOI: 10.1109/ICRA.2012.6225362

Hopping of a Monopedal Robot with a Biarticular Muscle Driven by Electromagnetic Linear Actuators

Yoshihiro Nakata, Atsuhiro Ide, Yutaka Nakamura,
Katsuhiro Hirata, *Member, IEEE* and Hiroshi Ishiguro, *Member, IEEE*

***Abstract*— The compliance of muscles with external forces and the structural stability given by biarticular muscles are important features of animals to realize dynamic whole body motions such as running and hopping in various environments. For this reason, we have been studying an electromagnetic linear actuator. This actuator can emulate the behavior of a human muscle such as the spring-damper characteristics by quick control of the output force (i.e. impedance control) and it is expected to be used as an artificial muscle. In this paper, we develop a monopedal robot possessing bi- and mono-articular muscles implemented by linear actuators. Thanks to the biarticular muscle, the bouncing direction of the robot can be controlled by changing the stiffness ellipse at the endpoint (i.e. foot) of the robot. We confirm that the bouncing direction of the robot can be controlled and hopping can be achieved by changing the stiffness ellipse.**

I. INTRODUCTION

Animals have great mobility, as they can move in various environments by performing whole body motions while coping with various disturbances such as running on a rough terrain or hopping over a ditch. There are two important mechanisms to realize such flexible motions. One is the compliance of muscles actuating the skeleton, and the other is the musculoskeletal structure itself [1]. The compliance of muscles enables animals to respond to external forces flexibly. The structure contributes to the stability of the whole body motion. For example, a biarticular muscle is a muscle which actuates two adjacent joints at the same time, modifying the effect of external forces on the whole body by changing its stiffness [2]. That is, the compliance characteristics at the end effector can be flexibly changed by utilizing a biarticular muscle. By responding to external forces with the proper stiffness at the end effector, animals can react to various disturbances and can make use of kinetic energy effectively.

In relation with the above properties, legged robots with artificial muscles including a biarticular muscle and their control mechanisms have been studied [3], [4]. Pneumatic actuators are widely used as artificial muscles for musculoskeletal robots due to their light weight and compliance properties induced by their physical character [5], [6]. For example, a legged "Athlete Robot" driven by pneumatic actuators can change the direction of the major axis of the stiffness ellipse [7]. Although the control of the bouncing direction can be achieved by presetting the stiffness ellipse, a quick change in stiffness during the robot's movement is difficult due to the slow response of the pneumatic actuators. Series elastic actuators (SEAs) are also used as variable compliance actuator for robots [8]. The structure of SEAs is simple and easy to implement in robots, but their response is also slow because the SEAs use a ball screw to actuate their mover. From the view point of compliance control, electric motors are suitable since they can change their output forces (or torques) quickly and arbitrarily according to the control inputs. The robots' easy and precise response to the external disturbances can be controlled by emitting an adequate force (or torque). Electric direct drive rotary motors are widely used to realize joints with compliant property, but there are two properties unfit for constructing a musculoskeletal robot. In order to implement a biarticular muscle, it is necessary to employ a complex mechanical structure such as a wired drive system [9] or a planetary gear [10]. Furthermore, external forces applied at the end effector directly act on the mover of the actuators, since they are a part of the skeletal system supporting its own body. This may cause them to break down especially when a strong impulsive force is generated by an accidental collision.

In this research, we use electromagnetic linear actuators as artificial muscles [11], because it is easy to implement multi-articular muscles. Also, they are not directly exposed to impulsive force since the skeletal system receives such forces and the actuators are used only for emitting output forces. We develop a monopedal (one-legged) robot which has bi- and mono-articular muscles implemented by electromagnetic linear actuators. The stiffness ellipse at the endpoint (foot) of the robot is controllable thanks to the biarticular muscle, and the robot can control its bouncing direction when it touches down to the ground. We employ a simple feedback control rule to change the stiffness ellipse at the end effector, i.e. foot, to make the robot hop repeatedly. Experimental results show that by using our method the robot can repeat hopping.

II. THE LEG MODEL WITH BIARTICULAR MUSCLES DRIVEN BY COMPLIANT ACTUATORS

In this section, we explain the leg model with biarticular muscles used in this research and how the stiffness ellipse at the foot changes according to the compliance of each actuator. We assume the monopedal robot is driven by elec-

This work was supported by Grant-in-Aid for JSPS Fellows (22-772).

Yoshihiro Nakata, Atsuhiro Ide, Yutaka Nakamura and Hiroshi Ishiguro are with Department of Systems Innovation, Graduate School of Engineering Science, Osaka University, 1-3 Machikaneyama, Toyonaka, Osaka, 560-8531, Japan {nakata.yoshihiro, ide.atsuhiro, nakamura, ishiguro}@is.sys.es.osaka-u.ac.jp

Katsuhiro Hirata is with Department of Adaptive Machine Systems, Graduate School of Engineering, Osaka University, 2-1 Yamadaoka, Suita, Osaka, 565-0871, Japan k-hirata@ams.eng.osaka-u.ac.jp

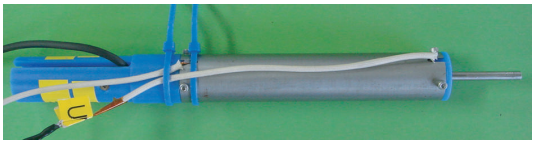

Fig. 1. Electromagnetic linear actuator

tromagnetic linear actuators, which can behave as a spring-damper system when it is controlled by a PD control thanks to its quick response. The characteristics of an emulated spring-damper, i.e., the natural length, elastic coefficient and viscosity coefficient, can be changed arbitrarily within the hardware limitations, according to the change of gain parameters of the PD controller.

A. Electromagnetic Linear Actuator

The electromagnetic linear actuator which we developed is a direct drive 3-phase synchronous linear motor [11]. There are 2 types of sensors. One measures the position of the mover (Inductcoder, Murata Machinery, Ltd.) and the other measures the current flow in each coil (PS-FBD 2/1 Module, dSPACE GmbH). By using these sensory inputs, it is able to calculate the target coil currents to generate an arbitrary given force for the current mover position. Fig. 1 shows our electromagnetic linear actuator (body length: 180mm, diameter: 20mm, stroke: 40mm and weight: 0.17kg) used in our experiment. The thrust of this actuator is 5.7N when the effective current is 1A. The physical properties of the actuator used in later simulations (Section IV) is set to those values.

B. Model of the Biological Muscle

Each joint of an animal is usually driven by an antagonistic pair of muscles (flexor and extensor muscles) because the biological muscles can only generate contractile force. Its impedance characteristics is determined by the balance of forces produced by these two muscles. A simplified model of the biological muscle is shown in Fig. 2 (left). The kinetic property of the simplified muscle model (i.e. when the contractile velocity is 0) can be represented as:

$$F_m = u - k(u)l, \tag{1}$$

where F_m, u, $k(u)$ and l are the total force generated by the muscle, the force generated by contractile element, the elastic coefficient of the muscle and the contractile length, respectively [12] (It is assumed that the elastic coefficient $k(u)$ is proportional to the contractile force u: $k(u) = k_0 u$ with a certain constant k_0). Note that the linear actuator can produce both contractile and extensive force and an antagonistic pair of muscles can be emulated and thus replaced by one actuator (See Fig. 2 (right)).

C. The Stiffness Ellipse at the Foot

A simplified model of the human leg with 3 antagonistic pairs of muscles is shown in Fig. 3. This model consists of 3 links with 2 joints and assumes the point foot. M_n denotes an antagonistic pair of muscles, where f_n and e_n

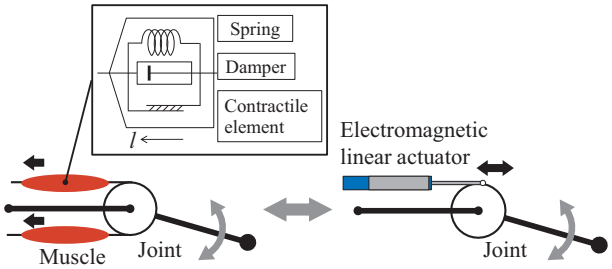

Fig. 2. Joint and muscle mechanisms

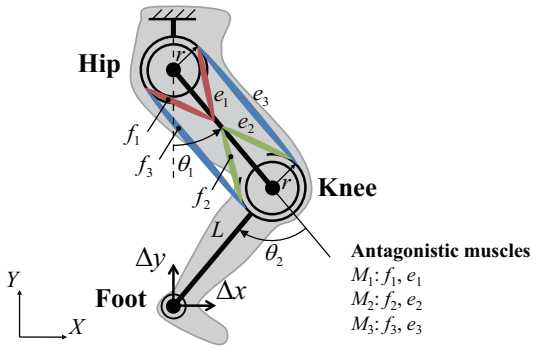

Fig. 3. Human leg model

are the flexor and extensor muscles, respectively. M_1 and M_2 are the monoarticular muscles at the hip and knee joint, respectively. M_3 is the biarticular muscles which is used to constrain the motion of the two joints. For simplicity, the moment arm of each joint has the same length r, and the lengths of both links (thigh and shank) are L. The elastic coefficient of f_n is assumed to be equal to that of e_n. The origin is set to the hip joint position. The potential energy ΔE_p at the foot is calculated as:

$$\Delta E_p = \begin{bmatrix} \Delta x & \Delta y \end{bmatrix} \mathbf{K} \begin{bmatrix} \Delta x & \Delta y \end{bmatrix}^T \tag{2}$$

where Δx and Δy are the horizontal and vertical axis components of the small displacement from the target position (equilibrium point) to the current endpoint, respectively. $\mathbf{K}$ is the stiffness matrix in Cartesian space formed as:

$$\mathbf{K} = \begin{bmatrix} C_{11} & C_{12} \\ C_{21} & C_{22} \end{bmatrix}^{-1} \tag{3}$$

where each element of compliance C_{ij} is defined as:

$$\left.\begin{aligned} C_{11} &= -\alpha^2 c_a - 2\alpha\gamma c_b - \gamma^2 c_c \\ C_{12} &= C_{21} = \alpha\beta c_a + (\alpha\delta + \beta\gamma) c_b + \gamma\delta c_c \\ C_{22} &= -\beta^2 c_a - 2\beta\delta c_b - \delta^2 c_c \end{aligned}\right\} \tag{4}$$

Variables α, β, γ and δ are defined as:

$$\left.\begin{aligned} \alpha &= -L\{\cos\theta_1 + \cos(\theta_1 - \theta_2)\} \\ \beta &= L\{\sin\theta_1 + \sin(\theta_1 - \theta_2)\} \\ \gamma &= -L\cos(\theta_1 - \theta_2) \\ \delta &= L\sin(\theta_1 - \theta_2) \end{aligned}\right\} \tag{5}$$

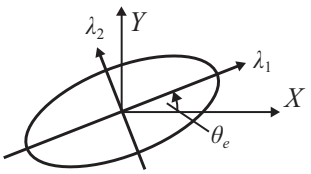

Fig. 4. Stiffness ellipse

The compliance c_a, c_b and c_c are defined as:

$$\left.\begin{array}{l} c_a = \frac{c_1(c_2+c_3)}{c_1+c_2+c_3} \\ c_b = -\frac{c_1 c_2}{c_1+c_2+c_3} \\ c_c = \frac{c_2(c_1+c_3)}{c_1+c_2+c_3} \end{array}\right\} \quad (6)$$

$$c_n = -\frac{1}{k_n(u_n) r^2} \qquad (n = 1, 2, 3) \quad (7)$$

Variables θ_1 and θ_2 are the angles of the hip and the knee joint, respectively. u_n, c_n and $k_n(u_n)$ are the sum of the antagonistic pair of muscles' contractile force, the compliance of the antagonistic pair of muscles, and the elastic coefficient of M_n, respectively.

By singular value decomposition, the stiffness matrix $\mathbf{K}$ is transformed as:

$$\mathbf{K} = \left[\begin{array}{cc} \boldsymbol{\nu}_1 & \boldsymbol{\nu}_2 \end{array}\right] \left[\begin{array}{cc} \lambda_1 & 0 \\ 0 & \lambda_2 \end{array}\right] \left[\begin{array}{cc} \boldsymbol{\nu}_1 & \boldsymbol{\nu}_2 \end{array}\right]^T \quad (8)$$

where $\lambda_{\{1,2\}}$ and $\boldsymbol{\nu}_{\{1,2\}}$ are eigenvalues and eigenvectors. $\mathbf{K}$ determines the characteristics of its corresponding stiffness ellipse (See Fig. 4) i.e., the volume ($\pi\lambda_1\lambda_2$), the shape (λ_1/λ_2), and the orientation ($\theta_e = \arg(\boldsymbol{\nu}_1)$). By changing these characteristics, the response of the robot against external forces can be changed.

III. CONTROL METHOD FOR THE MONOPEDAL ROBOT WITH A BIARTICULAR MUSCLE

In this section, we propose a control method based on changing the orientation of the stiffness ellipse. The robot can control its bouncing direction and its leg angle by adjusting the stiffness ellipse properly, depending on the angle of the leg when the robot touches down. In the simulation, the hopping motion of the robot controlled by our method is shown.

A. Adjustment of the Characteristics of the Stiffness Ellipse

The characteristics of the stiffness ellipse are determined from the coefficient of each muscle. In this analysis, the posture of the robot when it touches down is assumed to be fixed, and θ_1 and θ_2 are set to be 40deg and 80deg, respectively. The initial values of the elastic coefficients of all muscles are 600 N/m.

Fig. 5(a) shows the result when changing $k_1(u_1)$ ($k_2(u_2)$ and $k_3(u_3)$ are constant values in this figure). The stiffness ellipse rotates in a clockwise direction as $k_1(u_1)$ increases, and vice versa. Fig. 5(b) and 5(c) shows cases where $k_2(u_2)$ and $k_3(u_3)$ change. The stiffness ellipse does not rotate, but the length of the major axis is monotonically increased, as in $k_2(u_2)$. $k_3(u_3)$ has an opposite effect against $k_1(u_1)$.

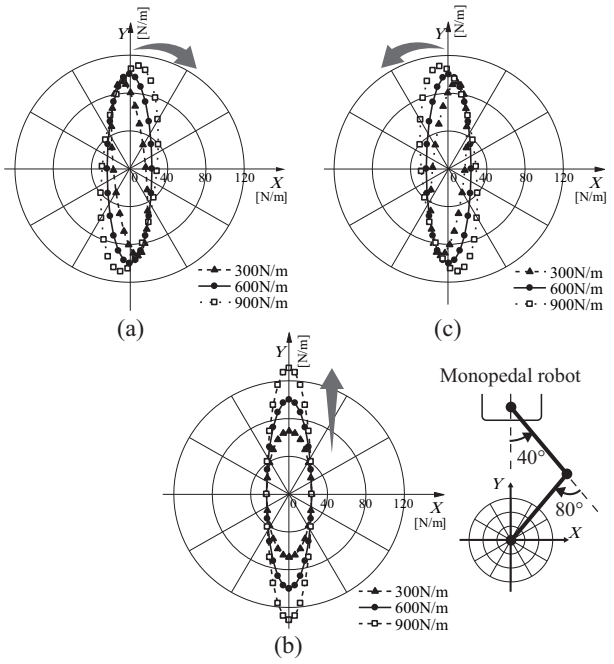

Fig. 5. Relationships between the stiffness ellipse and the elastic coefficient of each muscle

B. Control Method

The major and minor axes of the stiffness ellipse represent the directions of the large and small stiffness respectively. There are simple relationships: 1) the orientation of the stiffness ellipse is determined by the ratio between $k_1(u_1)$ and $k_3(u_3)$; 2) the length of the major axis is determined by changing $k_2(u_2)$. These relationships can be used to control the bouncing direction and angle of the leg of the monopedal robot.

Bouncing direction control (BDC)

When the major axis of the stiffness ellipse tilts forward (i.e. $k_1(u_1)$ is larger than $k_3(u_3)$), the robot is expected to jump forward, because the foot tends to move backward, and the robot tends to lean forward when it touches down. On the contrary, when the major axis of the stiffness ellipse tilts backward (i.e. $k_1(u_1)$ is smaller than $k_3(u_3)$), the robot is expected to jump backward. By changing $k_1(u_1)$ and $k_3(u_3)$ before it touches down, the monopedal robot can control its bouncing direction.

Leg angle control (LAC)

The leg angle is defined by the angle between the vertical direction and the line connecting the hip joint and foot as shown in Fig. 6. We assume that the center of gravity for the robot is at the hip joint. If the leg angle is not within a certain range, the robot goes down. However, the robot can change $k_1(u_1)$ and $k_3(u_3)$ (BDC) depending on the leg angle to maintain the proper leg angle. Details are described in the latter part of this paper.

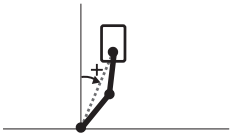

Fig. 6. Leg angle

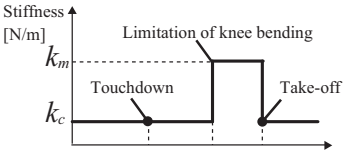

Fig. 7. Stiffness change ($A_{2,1}$,$A_{2,2}$)

Providing hopping energy

Since $k_2(u_2)$ does not change the bouncing direction, it is used to supply the energy lost during each hopping and make the robot hop repeatedly. Fig. 7 shows the variation of $k_2(u_2)$. $k_2(u_2)$ was set to be small during bending (k_c) and large during stretching the knee (k_m) in oder to maintain stable hopping.

C. Simulation of Hopping by the Monopedal Robot

The CAD model of the monopedal robot is shown in Fig. 8(a). The height from the foot to the hip is about 210mm (θ_1 =20deg and θ_2 =40deg) and the weight of whole robot is about 1.7kg (including the weight of the body 0.5kg). This robot model has a simulated touch sensor at the foot to detect the ground at touchdown (In the real robot, we implemented a touch sensor (FSR402, Interlink Electronics Inc.)). Three antagonistic pairs of muscles at the femoral area are replaced by four electromagnetic linear actuators. The placement of the actuators is shown in Fig. 8(b). Since the maximum isometric force of M_2 is nearly twice as large as M_1 and M_3 in the case of the human leg [13], [14], two actuators ($A_{2,1}$ and $A_{2,2}$) implemented at the front of the thigh act as a single muscle (M_2), controlled by the same control signal. One out of two actuators (A_1) implemented at the back of the thigh operates as M_1, while the other (A_3) operates as M_3. These actuators are implemented around the hip joint to maintain the center of gravity of the robot around the hip. The structure of joints is shown in Fig. 9. Each connection between a link and an actuator is made up of two linear sliders to maintain a constant moment arm. Since the current actuator cannot output enough thrust to jump under an environment with gravity acceleration, we employ a counter weight (See Fig. 15.), so that the effect of the gravity force is reduced. This equipment also makes the robot stable in radial and yaw directions. We set the gravity acceleration to g/3[m/s^2] (g=9.81m/s^2) because the experimental equipment reduces the effect of the gravity force. The movement of the trunk is restricted to translation in the horizontal and vertical directions (sagittal plain), in order to avoid the complexity of three-dimensional movements, i.e. the trunk does not rotate. In the simulation, the equations expressing the motions of the robot are derived and numerically calculated using the MATLAB/Simulink and SimMechanics toolbox [15]. Numerical integration was performed with a 4th order Runge—Kutta method. The simulation model considering the mass and inertia of the robot is shown in Fig. 8(c). The actual actuator has a friction different from that in the simulation, which was set by modifying the friction coefficient, i.e. the viscosity coefficient of the actuator model, considered to be 0.1Ns/m. The ground reaction force in the vertical direction generated between the foot and the floor was approximated by a nonlinear spring-damper model, and that in the horizontal direction is calculated as dynamic friction [16], [17].

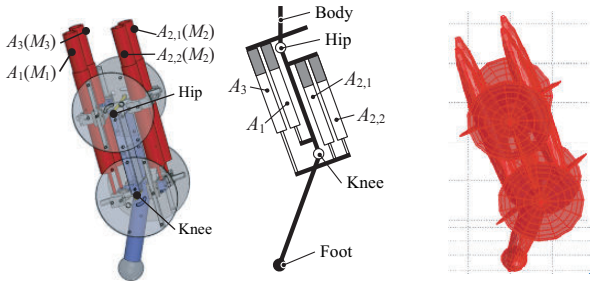

(a) CAD model (b) Placement of actuators (c) Simulation model

Fig. 8. Monopedal robot

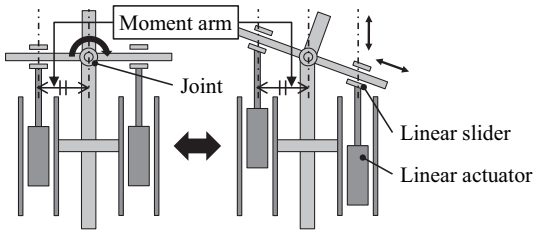

Fig. 9. Joint mechanism

Elastic coefficients and the bouncing direction

The bouncing direction when the robot with an initial posture falls down from its initial position is investigated. The elastic coefficients of the actuators, the initial position and the joint angles of the robot are shown in Table I. The bouncing direction is defined by the angle between the vertical direction and the moving direction of the hip joint as shown in Fig. 10. The simulation results are shown in Fig. 11(a). When the $k_1(u_1)$ is larger than $k_3(u_3)$, the robot tends to jump forward and vice versa. The elastic coefficients of $k_1(u_1)$ and $k_3(u_3)$ determine the bouncing direction and their relationship is almost linear. Therefore, the control rule for the bouncing direction using the stiffness control of the linear actuator is relatively simple. We also confirmed the following facts, shown in Fig. 11(a), about the robot without a biarticular muscle. Other simulation conditions are same. The result shows that this cannot jump backward, because the major axis of the stiffness ellipse can not tilted backward in the absence of a biarticular muscle. Thus, we can confirm that the biarticular muscle is important to determine the control of the bouncing direction of the robot.

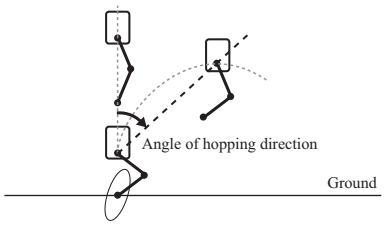

Fig. 10. Bouncing direction

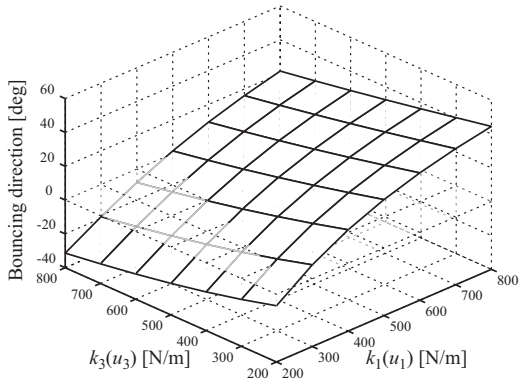

(a) Relationship between the elastic coefficients and the bouncing direction (with the biarticular muscle)

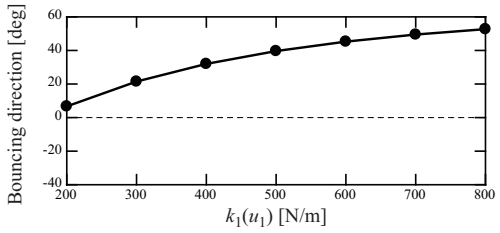

(b) Relationship between the elastic coefficient and the bouncing direction (with the biarticular muscle, $k_3(u_3) = 0$)

Fig. 11. Relationship between the elastic coefficients and the bouncing direction (Simulated result)

Leg angle control to prevent the robot falling down

During the hopping motion, the target length of each actuator is fixed. That is, the target leg angle of the robot is fixed. However, the leg angle of the robot changes because of the forces generated at touchdown or the take-off. To correct these errors we designed a simple control method of the leg angle based on the modification of the characteristics of the stiffness ellipse at touchdown. When the leg angle of the robot tilts forward (backward), the orientation of the stiffness ellipse is tilted backward (forward). With this control rule, it is expected that the leg angle of the robot can be modified. The conditions of the simulation are shown in Table II Fig. 12 show the relationships between θ_{td} and θ_{to}. θ_{td} and θ_{to} are the leg angles at touchdown and take-off, respectively. The initial posture of the robot is set to be tilted forward (Fig. 12(a)) or backward (Fig. 12(b)) with a certain height, and after that the robot falls down. This procedure (trial) is repeated several times. Since the initial posture of the robot varies by each trial and the angle of the leg changes during

TABLE I

SIMULATION CONDITIONS

Elastic coefficients of actuators	$k_1(u_1)$	200-800N/m (step size 50N/m)
	$k_3(u_3)$	200-800N/m (step size 50N/m)
	$k_2(u_2)$	500N/m (constant)
Initial position of the hip joint	x axis	0m
	y axis	0.25m
Initial joint angle of the robot	Hip joint θ_1	20deg
	Knee jointθ_1	40deg
Floor	y axis	0m

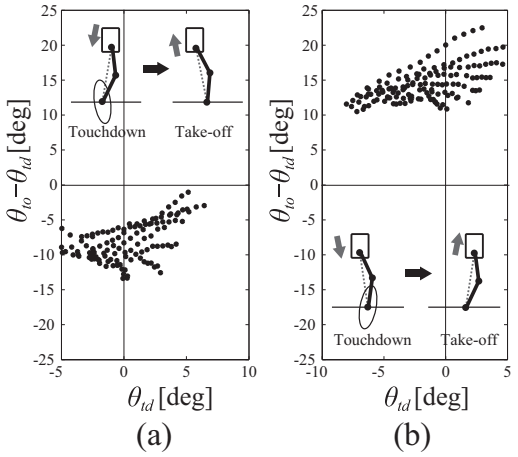

Fig. 12. Leg angle control (Simulation results)

the robot is falling down, it is not necessarily true that the leg angle at touchdown θ_{td} is always same. These figures show point diagrams of observed data whose horizontal and vertical axes show θ_{td} and $\theta_{to} - \theta_{td}$. When θ_{td} tilts forward with the orientation of the stiffness ellipse set to backward, θ_{to} rotates in the backward direction; conversely, if θ_{td} is tilted backward and the orientation of the stiffness ellipse is set to forward, then θ_{to} rotates in the forward direction. As the result, the angle of the leg tend to stay in a certain range.

Hopping of the monopedal robot with feedback control

In this simulation, the ground stiffness is changed according to the location at touchdown; as a result, the environment includes unexpected disturbances. It is we investigated whether the simple feedback control based on LAC can cope with such disturbances. The stiffness ellipse is changed

TABLE II

SIMULATION CONDITIONS

The orientation of the stiffness ellipse tilts backward	$k_1(u_1)$	200N/m
	$k_3(u_3)$	600N/m
	$k_2(u_2)$	k_c=200N/m, k_m=300N/m
The orientation of the stiffness ellipse tilts forward	$k_1(u_1)$	400N/m
	$k_3(u_3)$	200N/m
	$k_2(u_2)$	k_c=200N/m, k_m=300N/m
Floor	y axis	0m

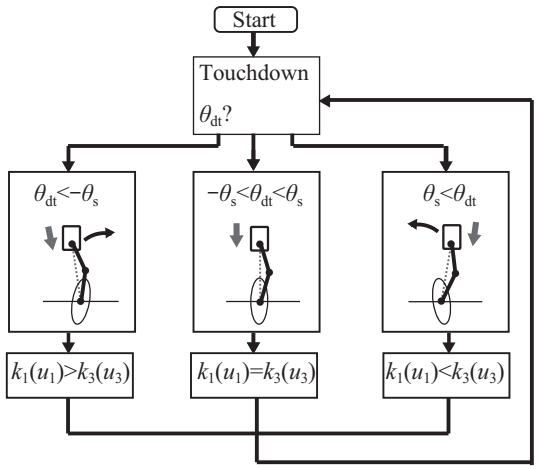

Fig. 13. Flowchart of the feedback control

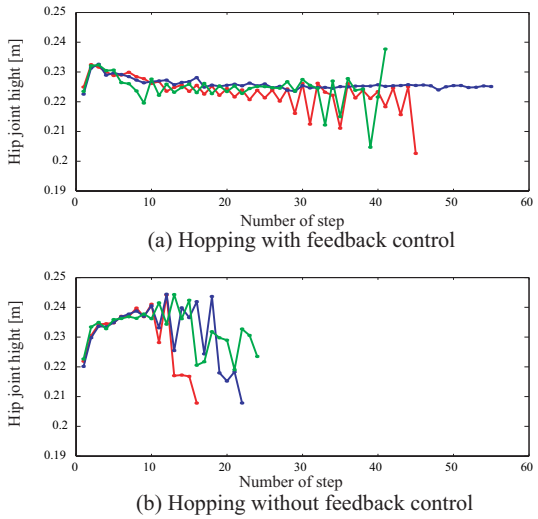

(a) Hopping with feedback control

(b) Hopping without feedback control

Fig. 14. Hip joint hight in each step (Simulation results)

according to the leg angle at touchdown. Fig. 13 shows the flowchart of the feedback control. Not that the leg angle is calculated according to position data of each actuator. θ_s is the threshold value ($\theta_s > 0$). The conditions of the simulation are shown in Table III.

14(a) shows the maximum hip joint hight in each step. 14(b) shows the result of the hopping without feedback control ($k_1(u_1)$ and $k_3(u_3)$ are constant). There are 3 different grand conditions (red, green and blue lines). The ground spring constant is changed depending on the position of the robot. From these figures, the robot can hop more than 40 steps by the feedback control. These simulation results indicate our control method works well.

IV. HOPPING OF THE MONOPEDAL ROBOT BY SIMPLE COMPLIANCE CONTROL

Fig. 15 shows the monopedal robot we developed and the experimental setup. In these experiments, the actuator $A_{2,1}$ is removed and three electromagnetic linear actuators are implemented on the robot, due to the shortage in the

TABLE III
SIMULATION CONDITIONS

Hopping with feedback control		
$\theta_{td} < -\theta_s$	$k_1(u_1)$	700N/m
	$k_3(u_3)$	300N/m
	$k_2(u_2)$	k_c=100N/m, k_m=380N/m
$-\theta_s < \theta_{td} < \theta_s$	$k_1(u_1)$	300N/m
	$k_3(u_3)$	300N/m
	$k_2(u_2)$	k_c=100N/m, k_m=380N/m
$\theta_{td} > \theta_s$	$k_1(u_1)$	200N/m
	$k_3(u_3)$	800N/m
	$k_2(u_2)$	k_c=100N/m, k_m=380N/m
	θ_s	1deg
Hopping without feedback control		
	$k_1(u_1)$	660N/m
	$k_3(u_3)$	300N/m
	$k_2(u_2)$	k_c=100N/m, k_m=380N/m
Floor	y axis	0m

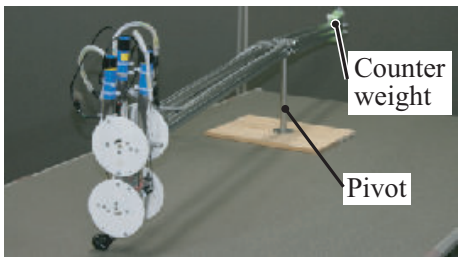

Fig. 15. Experimental setup

output capacity of the power supply. Although the maximum force applied to the knee joint is smaller, it is sufficient for investigating the effect of the stiffness ellipse, since this actuator does not change the direction of the long axis of the ellipse. The system configuration is shown in Fig. 16. The digital signal processor (dSPACE GmbH, MicroAutoBox and RapidPro System) calculates the target thrust of each actuator and the target current for each coil when generating the target thrust. The I/O unit outputs the input voltage to the coil of each actuator. The mover of the actuator is measured by the built-in linear encoder. Four markers are attached on the hip joint, the thigh, the knee joint and the foot to measure the motion of the robot. The position of the makers is measured by a motion capture system (Motion Analysis Corporation, MAC3D System).

A. Elastic Coefficients and Bouncing Direction

Bouncing directions are recorded when the robot falls down from the initial position. The height of the hip joint of the initial position is about 0.3m. θ_1 and θ_2 are set about 7deg and 14deg, respectively. Fig. 17 shows the measured result of the relationship between the elastic coefficient and the bouncing direction by changing the $k_1(u_1)$ and $k_3(u_3)$. In this figure, we can notice a similar tendency to the one shown in Fig. 11.

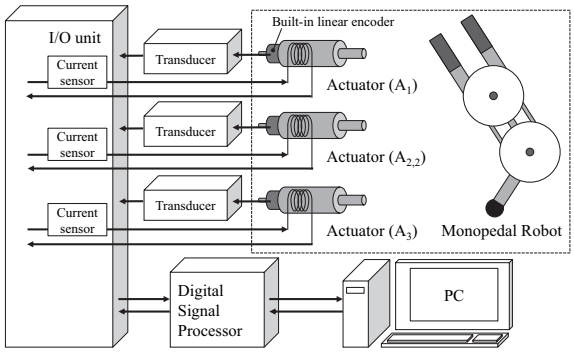

Fig. 16. System configuration

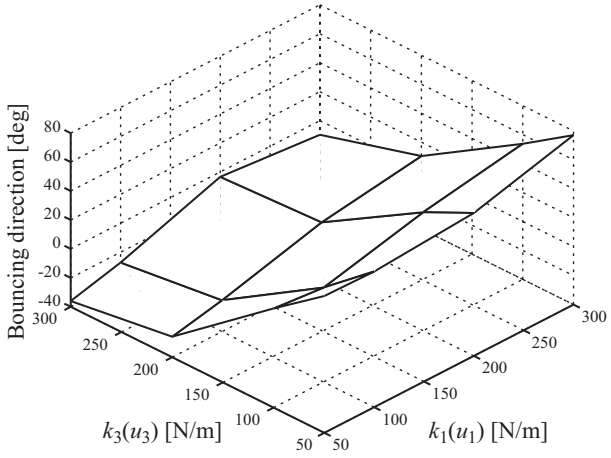

Fig. 17. Relationship between the elastic coefficients and the bouncing direction (Measured result)

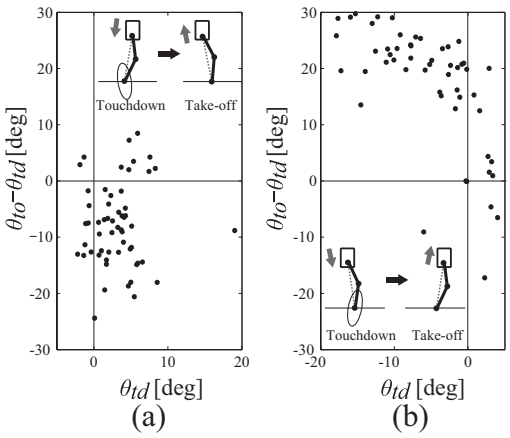

Fig. 18. Leg angle control (Measured results)

TABLE V
EXPERIMENTAL CONDITIONS

$\theta_{td} < -\theta_s$	$k_1(u_1)$	150N/m
	$k_3(u_3)$	100N/m
	$k_2(u_2)$	k_c=3N/m, k_m=300N/m
$-\theta_s < \theta_{td} < \theta_s$	$k_1(u_1)$	100N/m
	$k_3(u_3)$	100N/m
	$k_2(u_2)$	k_c=3N/m, k_m=300N/m
$\theta_{td} > \theta_s$	$k_1(u_1)$	100N/m
	$k_3(u_3)$	150N/m
	$k_2(u_2)$	k_c=3N/m, k_m=300N/m
	θ_s	1deg

Leg angle control

The experimental conditions are shown in Table IV Fig. 18 show the relationships between θ_{td} and θ_{to}. The initial posture of the robot is set to be tilt forward (Fig. 18(a)) or backward (Fig. 18(b)) with a certain height, and the robot falls down. These figures show point diagrams of observed data whose horizontal and vertical axes show θ_{td} and $\theta_{to}-\theta_{td}$ These figures show a similar tendency to that illustrated by 12(a) and (b). Thus, we can say that we were able to prevent the real robot from falling down by using LAC.

B. Hopping of the real robot with feedback control

We employ the simple feedback control based on LAC to realize hopping using a real robot. The conditions of the experiment are shown in Table. V. Fig. 19 shows the part of the motion sequences of the robot. The robot achieved 11 hopping steps before it falls down. When the stiffness ellipse does not change according to the leg angle of the robot, the robot hopped only 6 steps at most in our experiments. This may be because the robot could not maintain the leg angle properly to continue hopping. This experimental results indicate our control method works well. Also, it seems that jumping in backward direction is more difficult than jumping in forward direction due to the system's hardware limitations. It is important to note that the use of biarticular muscle reduces the computational cost. Even if there is no biarticular muscle, output force equivalent to the one generated by the stiffness ellipse based control can be generated according to the accurate estimate of the posture of the robot at each control cycle, but it requires a rapid control cycle, because the posture changes rapidly. However, in our robot, it can be controlled by making each actuator to emulate a simple spring, which basically means that each actuator is controlled by a simple P control with a fixed target length.

TABLE IV
EXPERIMENTAL CONDITIONS

The orientation of the stiffness ellipse tilts backward	$k_1(u_1)$	50N/m
	$k_3(u_3)$	300N/m
	$k_2(u_2)$	k_c=3N/m, k_m=200N/m
The orientation of the stiffness ellipse tilts forward	$k_1(u_1)$	150N/m
	$k_3(u_3)$	100N/m
	$k_2(u_2)$	k_c=3N/m, k_m=320N/m

V. CONCLUSION

In this research, we investigated a monopedal robot with a biarticular muscle. The stiffness ellipse before touchdown in each step can be set by utilizing the quick response of the electromagnetic linear actuator.

We confirmed that the robot with a biarticular muscle jumped forward and backward by adjusting the orientation

Fig. 19. Hopping of the monopedal robot

of the stiffness ellipse. On the contrary, the robot without a biarticular muscle could not jump backward. We also confirmed that the robot with a biarticular muscle can recover its posture by controlling the bouncing direction. It seems that biarticular muscles contribute to improving the controllability and stability of the dynamical whole body motion.

Our monopedal robot hop more steps using our simple feedback control method which determines the characteristics of the stiffness ellipse. In this method, the orientation of the stiffness ellipse before touchdown is adjusted according to a simple rule and the system does not require large amount of computational power. Nevertheless, it succeeds in improving the stability and robustness against disturbance.

In this study, the foot, ankle joint and rotation of the body are not considered. We will confirm the effect of biarticular muscles in controlling the stiffness ellipse to realize stable hopping motion in more realistic conditions in the future.

In a wide range of locomotion researches, the running and hopping motions of animals are explained employing the Spring Loaded Inverted Pendulum (SLIP) model [18]. This model uses the point-mass body and spring-like leg, but it does not explain the compliance characteristics of the leg using the stiffness ellipse. It seems to be useful to improve our method using this idea.

REFERENCES

[1] N. Hogan, "Adaptive Control of Mechanical Impedance by Coactivation of Antagonist Muscles", *IEEE Transactions on Automatic Control*, vol.29, no.8, 1984, pp.681—690.

[2] G. J. van Ingen Schenau, "From rotation to translation: Constraints on multi-joint movements and the unique action of bi-articular muscles", *Human Movement Science,*, vol.8, no.4, 1989, pp.301-337.

[3] F. Iida, J. Rummel and A. Seyfarth, "Bipedal walking and running with spring-like biarticular muscles", *Journal of Biomechanics*, vol.41, no.3, 2008, pp.656-667.

[4] K. Hosoda, Y. Sakaguchi, H. Takayama and T. Takuma, "Pneumatic-driven jumping robot with anthropomorphic muscular skeleton structure", *Autonomous Robots*, vol.28, no.3, 2009, pp.307-316.

[5] M. Wisse and R. Q. van der Linde, *Delft Pneumatic Bipeds*, Springer Tracts in Advanced Robotics, vol.34, Springer-Verlag, 2007, ch.3.

[6] B. Vanderborght, *Dynamic Stabilisation of the Biped Lucy Powered by Actuators with Controllable Stiffness*, Springer Tracts in Advanced Robotics, vol.63, Springer-Verlag, 2010, ch.2.

[7] R. Niiyama and Y. Kuniyoshi, "Design principle based on maximum output force profile for a musculoskeletal robot", *Industrial Robot: An International Journal*, vol.37, no.3, 2010, pp.250-255.

[8] G. A. Pratt, "Legged robots at MIT: what's new since Raibert?", *IEEE Robotics & Automation Magazine*, vol.7, no.3, 2000, pp.15-19.

[9] I. Mizuuchi, Y. Nakanishi, Y. Sodeyama, Y. Namiki, T. Nishino, N. Muramatsu, J. Urata, K. Hongo, T. Yoshikai and M. Inaba, "An Advanced Musculoskeletal Humanoid Kojiro", *in Proceedings of the 2007 IEEE-RAS International Conference on Humanoid Robots*, 2007.

[10] Y. Kimura, O. Sehoon and Y. Hori, "Novel robot arm with bi-articular driving system using a planetary gear system and disturbance observer", *11th IEEE International Workshop on Advanced Motion Control*, 2010, pp.296-301.

[11] Y. Nakata, H. Ishiguro and K. Hirata, "Dynamic Analysis Method for Electromagnetic Artificial Muscle Actuator under PID Control", *in Proceedings of the 17th Conference on the Computation of Electromagnetic Fields*, 2009, pp.664-665.

[12] Carol Y. Scovil, Janet L. Ronsky, "Sensitivity of a Hill-based muscle model to perturbations", *Journal of Biomechanics*, vol39, no.11, 2006, pp.2055-2063.

[13] I. C. Wright, R. R. Neptune, A. J. van den Bogert and B. M. Nigg, "Passive regulation of impact forces in heel-toe running", *Clinical Biomechanics*, vol.13, no.7, 1998, pp.521-531.

[14] S. L. Delp, "Surgery simulation: A computer-graphics system to analyze and design musculoskeletal reconstructions of the lower limb", Stanford University, Ph.D. Thesis, 1990, ch.4.

[15] L. F. Shampine and M. W. Reichelt, *The MATLAB ODE Suite*, Natick, MA: The MathWorks, 1997.

[16] K. G. M. Gerritsen, A. J. van den Bogert and B. M. Nigg, "Direct dynamics simulation of the impact phase in heel-toe running", *Journal of Biomechanics*, vol.28, no.6, 1995, pp.661-668.

[17] A. J. van den Bogert, H. C. Schamhardt and A. Crowe, "Simulation of quadrupedal locomotion using a rigid body model", *Journal of Biomechanics*, vol.22, No.1, 1989, pp.33-41.

[18] R.J. Full and D.E. Koditschek, "Templates and anchors: neuromechanical hypotheses of legged locomotion on land", *Journal of Experimental Biology*, vol.202, 1999, pp.3325-3332.